

SCIENTIFIC REPORTS



OPEN

Red blood cell thickness is evolutionarily constrained by slow, hemoglobin-restricted diffusion in cytoplasm

Sarah L. Richardson & Pawel Swietach

Received: 22 June 2016

Accepted: 11 October 2016

Published: 25 October 2016

During capillary transit, red blood cells (RBCs) must exchange large quantities of CO_2 and O_2 in typically less than one second, but the degree to which this is rate-limited by diffusion through cytoplasm is not known. Gas diffusivity is intuitively assumed to be fast and this would imply that the intracellular path-length, defined by RBC shape, is not a factor that could meaningfully compromise physiology. Here, we evaluated CO_2 diffusivity (D_{CO_2}) in RBCs and related our results to cell shape. D_{CO_2} inside RBCs was determined by fluorescence imaging of $[\text{H}^+]$ dynamics in cells under superfusion. This method is based on the principle that H^+ diffusion is facilitated by $\text{CO}_2/\text{HCO}_3^-$ buffer and thus provides a read-out of D_{CO_2} . By imaging the spread of H^+ ions from a photochemically-activated source (6-nitroveratraldehyde), D_{CO_2} in human RBCs was calculated to be only 5% of the rate in water. Measurements on RBCs containing different hemoglobin concentrations demonstrated a halving of D_{CO_2} with every 75 g/L increase in mean corpuscular hemoglobin concentration (MCHC). Thus, to compensate for highly-restricted cytoplasmic diffusion, RBC thickness must be reduced as appropriate for its MCHC. This can explain the inverse relationship between MCHC and RBC thickness determined from >250 animal species.

The principal biological function of red blood cells (RBCs) is to exchange large volumes of O_2 and CO_2 during their brief (typically <1 s) transit through the microvasculature¹. The speed of gas turnover by RBCs is therefore a measure of their physiological fitness, and highly-conserved biological adaptations are expected to relate to faster gas exchange. The steps in the gas exchange cascade include gas permeation across the cell membrane and binding onto hemoglobin. Additionally in the case of CO_2 , gas molecules are converted reversibly to HCO_3^- ions (which are then transported by anion exchanger 1, AE1) plus H^+ ions (which are buffered by hemoglobin). These processes are coupled together by cytoplasmic diffusion. According to the prevailing consensus, efficiency of gas exchange is strongly dependent on protein-facilitated membrane transport, including AE1-assisted HCO_3^- transport and aquaporin1-assisted gas permeation^{2,3}.

A conserved and characteristic feature of human and animal RBCs is their flattened shape. The physiological relevance of this geometry has largely been attributed to the mechanical benefits it offers to circulating blood. RBC flattening allows microvasculature to co-evolve smaller luminal diameters and therefore maximize capillary density. In the case of human RBCs, the biconcave shape supports laminar flow and shear-thinning⁴, minimizes platelet scatter and atherogenic risk⁵, permits cells to squeeze through microvasculature^{6,7} and is the lowest energy-level that the cell returns to following deformation in capillaries^{8–11}. Elliptical or otherwise flattened RBCs of many non-human species may also manifest, to some degree, these mechanical benefits. Recently, cell geometry has been proposed as a stringent criterion by which splenic inter-endothelial slits select healthy RBCs for continued circulation¹², but it is unclear if similar criteria apply in non-human species. These aforementioned mechanical considerations do not, however, offer a unifying explanation for the wide range of RBC thicknesses observed naturally in different animal species, and its inverse relationship with mean corpuscular hemoglobin concentration (MCHC)^{13–15}. We postulate that RBC thickness and its relationship with MCHC may, instead, relate more closely to the efficiency of gas turnover.

Department of Physiology, Anatomy and Genetics, Oxford OX1 3PT, European Union, United Kingdom. Correspondence and requests for materials should be addressed to P.S. (email: pawel.swietach@dpag.ox.ac.uk)

Theoretically, the flattened RBC form may facilitate gas exchange in two ways. Firstly, it increases the cell's surface area/volume ratio (ρ), which allows faster membrane transport. Secondly, it collapses the path-length for cytoplasmic diffusion, which reduces the time delays associated with intracellular gas transport. In the case of human RBCs (major radius, r , of $4\ \mu\text{m}$), adapting the shape from a hypothetical sphere (volume $268\ \text{fl}$; surface area $200\ \mu\text{m}^2$) to a flattened form (volume $90\ \text{fl}$; surface area $136\ \mu\text{m}^2$) doubles ρ and hence transmembrane flux^{13–15}. The significance of this effect can be evaluated by considering the slowest membrane transport process, AE1-facilitated HCO_3^- transport, which has an apparent permeability constant³ (P_{m,HCO_3^-}) of $18\ \mu\text{m/s}$ and can be ascribed a time constant equal to $1/(\rho \times P_{m,\text{HCO}_3^-})$. The AE1-related time constant for the spherical geometry is $0.074\ \text{s}$, which is reduced to $0.037\ \text{s}$ for the flattened shape, yet both are compatible with equilibration during capillary transit. The biconcave shape of human RBCs reduces the mean cytoplasmic path-length to $0.9\ \mu\text{m}$ (equal to the cell's average half-thickness, h), which shortens intracellular diffusion time delays by a factor of seven, compared to a spherical RBC variant ($r^2/6 \div h^2/2$). However, this seven-fold acceleration will not translate into a meaningful improvement to gas exchange efficiency if gas diffusion coefficients are high, as they are in water. Paradoxically, gas diffusivity inside gas-carrying RBCs has not been measured, but is intuitively assumed to be rapid. Indeed, O_2 and CO_2 diffusivity measurements in hemoglobin solutions and hemolysates ($\sim 10^3\ \mu\text{m}^2/\text{s}$) appear to support this assertion^{2,14,16}. At this magnitude of diffusivity, cytoplasmic path-length and cell shape are *not* expected to be critical for determining the efficiency of gas exchange. In summary, our current understanding of RBC physiology predicts only a modest advantage of the flattened RBC shape for gas exchange, but this inference is based on an indirect characterization of gas transport inside the RBC.

In this study, we revisited the notion that gases diffuse rapidly in RBC cytoplasm. The required experimental approach must be capable of resolving diffusion on the scale of a single intact cell, and exclude contributions from permeation across extracellular unstirred layers and the surface membrane. To meet these criteria, we evaluated CO_2 diffusivity (D_{CO_2}) in intact RBCs by measuring the ability of $\text{CO}_2/\text{HCO}_3^-$ to facilitate cytoplasmic H^+ diffusion^{17–19}. This measurement method is based on the observation that cytoplasmic H^+ ions are heavily buffered²⁰, and therefore diffuse only as fast as the buffers there are bound to (with essentially no free ion movement)^{21,22}. Thus, by determining the $\text{CO}_2/\text{HCO}_3^-$ -dependent component of buffer-facilitated H^+ diffusion^{17,18,23}, it is possible to quantify D_{CO_2} . Our measurements on human RBCs demonstrate substantially restricted CO_2 diffusivity, to 5% of the rate in water, which is an order of magnitude slower than estimates made previously in cell-free hemoglobin solutions. By imaging osmotically-swollen human RBCs (to dilute MCHC) and RBCs from species with different hemoglobin concentrations, we demonstrate that D_{CO_2} decreases sharply with MCHC, consistent with hemoglobin-imposed tortuosity to small-molecule diffusion. We conclude that diffusion across cytoplasm is a hitherto unrecognized rate-limiting step for gas exchange which imposes a critical limit on the RBC thickness, beyond which physiological function becomes inefficient and incomplete. In particular, the full manifestation of the Bohr Effect²⁴ (i.e. the process by which hemoglobin releases O_2 at acidic vascular beds) is attainable only in RBCs that are adequately thin because the underlying H^+ trigger is transmitted intracellularly by slow $\text{CO}_2/\text{HCO}_3^-$ diffusion. Highly restricted cytoplasmic diffusivity can explain the inverse RBC thickness/MCHC relationship observed amongst different animal species, and highlights the potential vulnerability of gas exchange efficiency in diseases that involve a change in RBC shape, such as in spherocytosis.

Results

Using measurements of spatio-temporal $[\text{H}^+]$ dynamics as a read-out of CO_2 diffusion. CO_2 cannot be imaged dynamically inside a single intact RBC, but its acidic chemistry allows pH-sensitive fluorescent dyes, such as cSNARF1²⁰, to monitor its diffusion. H^+ ions are highly buffered in cells, therefore their apparent cytoplasmic diffusivity ($D_{\text{H}^+}^{\text{app}}$) is determined exclusively by the mobility of H^+ -carrying buffers (Fig. 1A,B)^{21,22}. Based on this biophysical principle, it is possible to describe the diffusive properties of cytoplasmic buffers from measurements of H^+ dynamics in intact cells^{18,25}. To determine $D_{\text{H}^+}^{\text{app}}$, a local source of H^+ ions was produced in cytoplasm by photolytic uncaging from the membrane-permeant H^+ -donor 6-nitroveratraldehyde (NVA)²³ once every $0.13\ \text{s}$. This generates an acidic microdomain which dissipates at a rate determined by the buffers' concentrations, reaction kinetics with H^+ ions, and diffusion coefficients. To follow the progress of buffer-facilitated H^+ diffusion, pH-sensitive cSNARF1 fluorescence was imaged confocally across the RBC's horizontal plane at intervals between H^+ uncaging (e.g. Fig. 1C,D)²⁰. Provided that membrane transport of H^+ and HCO_3^- ions is slow or inactivated, best-fitting these spatio-temporal $[\text{H}^+]$ data with a diffusion equation (derived previously^{18,23,26}) gives a robust measure of $D_{\text{H}^+}^{\text{app}}$.

During experiments, continuous superfusion of cells controls for temperature and $\text{CO}_2/\text{HCO}_3^-$ concentration²⁰. In RBCs superfused with $\text{CO}_2/\text{HCO}_3^-$ -free solution, H^+ diffusion is facilitated solely by hemoglobin (Fig. 1A). Under these conditions, $D_{\text{H}^+}^{\text{app}}$ reports H^+ diffusion facilitated by the translation and rotation of hemoglobin molecules²⁷. When RBCs are superfused with $\text{CO}_2/\text{HCO}_3^-$ -containing solution, cytoplasmic diffusion of H^+ ions is additionally facilitated by $\text{CO}_2/\text{HCO}_3^-$, thus $D_{\text{H}^+}^{\text{app}}$ reports the combined effects of hemoglobin and $\text{CO}_2/\text{HCO}_3^-$ (Fig. 1B). Since these two buffer-shuttles are additive, the effect on $D_{\text{H}^+}^{\text{app}}$ of introducing $\text{CO}_2/\text{HCO}_3^-$ into cytoplasm is a read-out of the turnover of the $\text{CO}_2/\text{HCO}_3^-$ buffer-shuttle. High carbonic anhydrase (CA) activity in RBCs ensures that the $\text{CO}_2/\text{HCO}_3^-$ buffer-shuttle is *not* meaningfully rate-limited by chemical reactions; instead, $\text{CO}_2/\text{HCO}_3^-$ -facilitated H^+ diffusion is strongly dependent on the cytoplasmic diffusion coefficients of CO_2 gas and HCO_3^- ions (D_{CO_2} , $D_{\text{HCO}_3^-}$). Thus, the first step in quantifying D_{CO_2} and $D_{\text{HCO}_3^-}$ is to probe the $\text{CO}_2/\text{HCO}_3^-$ -dependent and independent components of $D_{\text{H}^+}^{\text{app}}$.

$\text{CO}_2/\text{HCO}_3^-$ weakly facilitates cytoplasmic H^+ diffusion in the cytoplasm of human RBCs. $\text{CO}_2/\text{HCO}_3^-$ -independent $D_{\text{H}^+}^{\text{app}}$ was measured in human RBCs superfused at $37\ ^\circ\text{C}$ with $\text{CO}_2/\text{HCO}_3^-$ -free normal Tyrode (0NT) solution containing $1\ \text{mM}$ NVA. Photolysis acidifies the cytoplasm at $\sim 0.1\ \text{pH}$ units/s, therefore $D_{\text{H}^+}^{\text{app}}$ measurements correspond to a mildly acid-shifted cytoplasmic pH (pH_c). To probe $D_{\text{H}^+}^{\text{app}}$ over a range

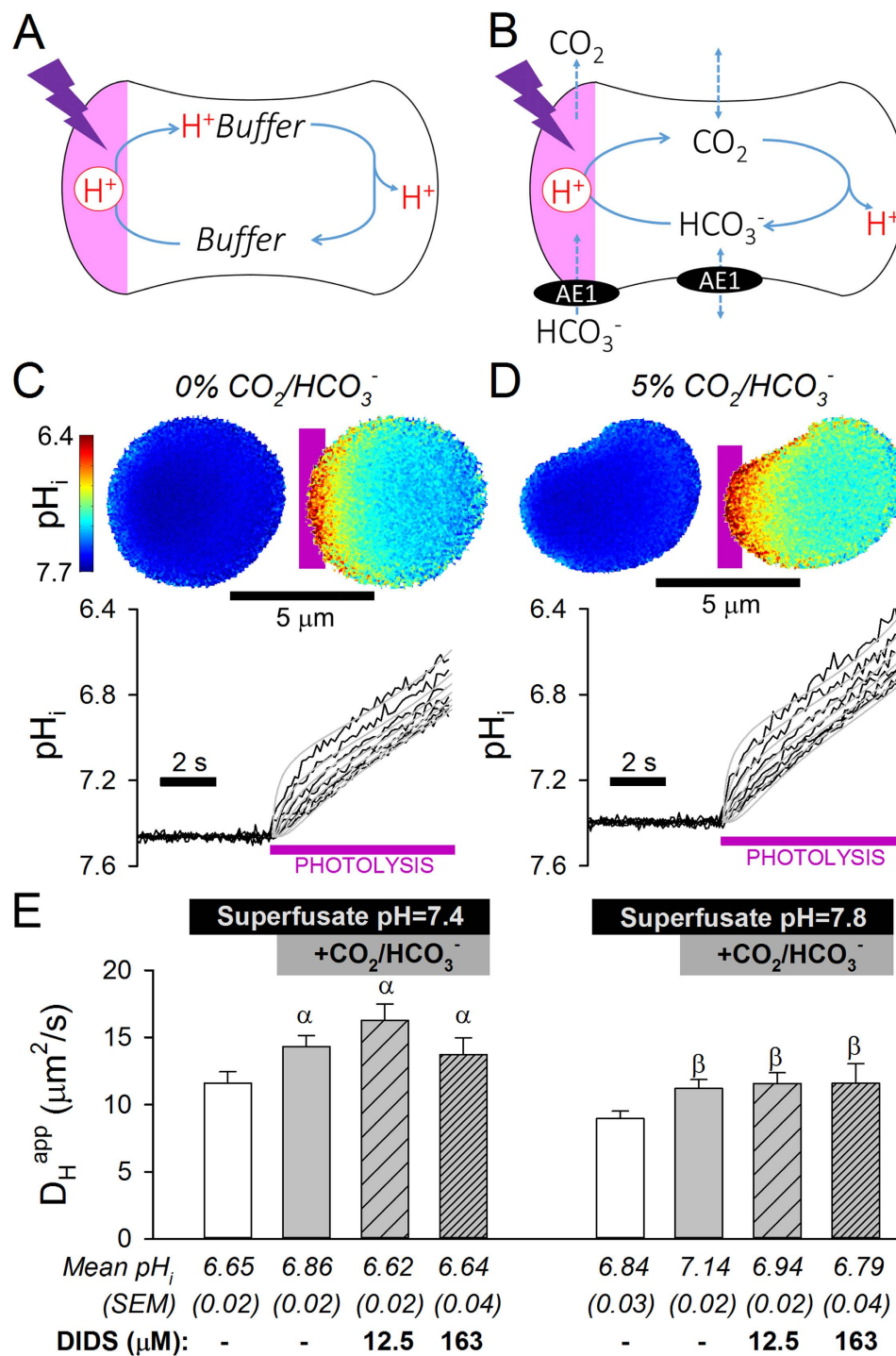


Figure 1. H^+ mobility in the cytoplasm of human RBCs is a read-out of $\text{CO}_2/\text{HCO}_3^-$ diffusivity. (A) Buffer (e.g. hemoglobin) facilitated H^+ diffusion from a local H^+ -uncaging site (photolysis of 6-nitroveratraldehyde). (B) H^+ diffusion facilitated additionally by $\text{CO}_2/\text{HCO}_3^-$. Membrane HCO_3^- permeability is set by AE1 (anion exchanger 1) activity. (C) Human RBC superfused in $\text{CO}_2/\text{HCO}_3^-$ -free buffer (at pH 7.8). H^+ ions diffuse slowly from uncaging site, as shown by maps of intracellular pH (pH_i) before and after 2 s of uncaging and pH_i time courses in regions of interest (ROIs) at increasing distance from the uncaging site. The width of each ROI was $1/10^{\text{th}}$ of RBC's major diameter; data for ROIs 1 (uncaging site), 2, 3, 4, 5, 6 and 8 shown. Grey curves are best fit using a diffusion equation. (D) Experiment on RBCs superfused with 5% $\text{CO}_2/\text{HCO}_3^-$ (at pH 7.8). The diffusion equation is solved using the finite element method which takes fully into account differences in cell outline, as observed between the cells shown in panels C and D. (E) Apparent H^+ diffusion coefficients ($D_{\text{H}}^{\text{app}}$; mean \pm SEM of 10–35 cells), showing the small effect of the $\text{CO}_2/\text{HCO}_3^-$ buffer-shuttle. Where indicated, DIDS was added to block AE1. Symbols α and β denote significance ($P < 0.05$; $P < 0.02$) compared to measurements in the absence of $\text{CO}_2/\text{HCO}_3^-$.

that encompasses physiological pH_c , experiments were performed in superfusates at pH 7.4 or 7.8. Membrane transport of HCO_3^- by AE1 is largely inactivated in the absence of $\text{CO}_2/\text{HCO}_3^-$, therefore uncaged H^+ ions are retained in cytoplasm. Figure 1C shows the slow spread of H^+ ions through the cytoplasm of a human RBC in the absence of $\text{CO}_2/\text{HCO}_3^-$. Measured $D_{\text{H}^{\text{app}}}$ (Fig. 1E) was three orders of magnitude slower than in water ($1.2 \times 10^4 \mu\text{m}^2/\text{s}$)²⁸. Immature RBCs, or reticulocytes, have been proposed to contain small histidine derivatives, such as carnosine²⁹, which could facilitate H^+ diffusion alongside hemoglobin. However, $D_{\text{H}^{\text{app}}}$ in cells identified positively by Thiazole Orange staining as reticulocytes was no different to $D_{\text{H}^{\text{app}}}$ in Thiazole Orange-negative (mature) RBCs (Fig. S1). Thus, the concentration of small-molecule histidine derivatives in reticulocytes is not sufficient to meaningfully influence H^+ diffusivity.

Next, experiments were performed on RBCs superfused with $\text{CO}_2/\text{HCO}_3^-$ -buffered NT (BNT) containing 5% CO_2 and either 22 mM HCO_3^- (for pH 7.4) or 55 mM HCO_3^- (for pH 7.8; Fig. 1D; solution osmolality was corrected to 296 mOsm/kg by balancing [NaCl]). If D_{CO_2} were rapid, the $\text{CO}_2/\text{HCO}_3^-$ buffer-shuttle would accelerate $D_{\text{H}^{\text{app}}}$ substantially and collapse pH gradients; however, introducing $\text{CO}_2/\text{HCO}_3^-$ into cytoplasm increased $D_{\text{H}^{\text{app}}}$ by only 2–3 $\mu\text{m}^2/\text{s}$ (Fig. 1E), indicating that $\text{CO}_2/\text{HCO}_3^-$ has a limited capacity to facilitate H^+ diffusion, comparable to that of hemoglobin. Activation of AE1 in $\text{CO}_2/\text{HCO}_3^-$ -containing superfusates may, in principle, compromise the accuracy of $D_{\text{H}^{\text{app}}}$ measurements. However, $D_{\text{H}^{\text{app}}}$ estimates were unaffected by blocking AE1 with 12.5 μM or 163 μM 4,4'-diisothiocyano-2,2'-stilbenedisulfonic acid (DIDS; Fig. 1E), indicating that the magnitude of membrane HCO_3^- transport is not sufficient to short-circuit the cytoplasmic $\text{CO}_2/\text{HCO}_3^-$ buffer-shuttle (NB: even the lower dose of DIDS was sufficient to inhibit AE1; Fig. S2). Cytoplasmic CA activity was not inactivated by DIDS, NVA or its photolytic derivative (Fig. S3), therefore low $D_{\text{H}^{\text{app}}}$ was not an erroneous result of inhibited $\text{CO}_2/\text{HCO}_3^-$ reaction kinetics.

Solute diffusion in RBC cytoplasm is restricted by the high concentration of hemoglobin. To investigate if slow cytoplasmic diffusivity is unique to $\text{CO}_2/\text{HCO}_3^-$, the mobility of calcein (a fluorescent marker) was measured in intact human RBCs. Applying a high-intensity laser beam every 0.13 s to one end of the cell bleaches calcein locally, and drives a diffusive redistribution of fluorescence signal, which was imaged throughout the cell at intervals between bleaching events. Time delays in calcein fluorescence measured at different distances from the bleaching region provide a readout of cytoplasmic diffusivity (D_{calc}), measured to be $47.8 \pm 5.95 \mu\text{m}^2/\text{s}$, i.e. 13-fold lower than in water ($\sim 600 \mu\text{m}^2/\text{s}$)³⁰ (Fig. 2A). This result indicates that RBC cytoplasm is a highly tortuous environment for diffusion.

Hemoglobin, which occupies a quarter of human RBC volume²⁰, is likely to impose a substantial tortuosity to the movement of solutes in cytoplasm. Loosening hemoglobin density is expected to accelerate small-molecule diffusion, and this was tested in osmotically-swollen cells (Fig. 2B). RBCs were first pre-equilibrated in, and then superfused with 155 or 220 mOsm/kg solutions (prepared by reducing [NaCl]). In the absence of $\text{CO}_2/\text{HCO}_3^-$, cytoplasmic dilution increased $D_{\text{H}^{\text{app}}}$ (Fig. 2C), presumably because of less restricted translational and rotational movements of H^+ -carrying hemoglobin molecules²⁷. The relationship between $D_{\text{H}^{\text{app}}}$ and osmolality was steeper after introducing a constant concentration of $\text{CO}_2/\text{HCO}_3^-$ into cytoplasm (Fig. 2C). This finding indicates that at lower hemoglobin density, $\text{CO}_2/\text{HCO}_3^-$ is more effective in facilitating H^+ diffusion. This occurs despite CA activity dilution, adding further evidence that H^+ diffusion is not reaction-limited (i.e. even after 2-fold dilution, CA activity remains very high).

To explore the effect of naturally occurring differences in hemoglobin concentration on $D_{\text{H}^{\text{app}}}$, measurements were performed on RBCs from chicken, alpaca and *Xenopus* (Fig. 3A–C). Previous studies have detected carnosine in nucleated erythrocytes³¹, which may augment $D_{\text{H}^{\text{app}}}$ in chicken and *Xenopus* RBCs by acting as a mobile buffer alongside hemoglobin and $\text{CO}_2/\text{HCO}_3^-$. However, using a modification of Pauly's assay, levels of small-molecule histidine derivatives were in the sub-millimolar range, with the highest levels detected in chicken RBCs (0.5 mM; Fig. S4). Over this low concentration range, histidine-containing small molecules cannot meaningfully increase $D_{\text{H}^{\text{app}}}$, therefore hemoglobin and $\text{CO}_2/\text{HCO}_3^-$ remain the principal H^+ -carriers. To measure $D_{\text{H}^{\text{app}}}$, alpaca and chicken RBCs were superfused in solution at 37 °C and pH 7.8, whereas *Xenopus* cells were superfused at room temperature and pH 7.5 to match their normal physiology. Nuclear regions in *Xenopus* and chicken RBCs were excluded in the analysis of pH (Hoechst 33342-positive nuclear areas also had higher intensity of cSNARF1 fluorescence, likely reflecting the ambient physicochemical environment of nucleoplasm; Fig. S5). Compared to human RBCs, chicken and *Xenopus* RBCs are larger and have a lower MCHC, whereas alpaca RBCs are smaller but with higher MCHC (Table S1). High CA activity was detected in hemolysates from all species studied, although it was lower in alpaca and *Xenopus* compared to humans (Fig. S6). Introducing $\text{CO}_2/\text{HCO}_3^-$ into cytoplasm increased $D_{\text{H}^{\text{app}}}$ in RBCs from chicken and *Xenopus*, but not alpaca (Fig. 3D). Hypotonic swelling (i.e. loosening hemoglobin density) increased $D_{\text{H}^{\text{app}}}$ further in chicken and alpaca RBCs (NB: *Xenopus* RBC are too fragile for this experiment). Figure 3E summarizes the relationship between $D_{\text{H}^{\text{app}}}$ and MCHC; with the exception of cold-blooded *Xenopus*, all data-points followed an exponentially-declining relationship. In summary, the facilitatory effect of $\text{CO}_2/\text{HCO}_3^-$ on $D_{\text{H}^{\text{app}}}$ was attenuated at higher MCHC, consistent with hemoglobin-imposed tortuosity.

Calculated CO_2 diffusivity in cytoplasm is slow and dependent on hemoglobin concentration.

Cytoplasmic H^+ diffusivity is related mathematically^{21,22} to the concentration, mobility and protonation/deprotonation kinetics of hemoglobin and $\text{CO}_2/\text{HCO}_3^-$. In this system, all variables except for $\text{CO}_2/\text{HCO}_3^-$ mobility (D_{CO_2} , D_{HCO_3}), are known, therefore an algorithm can be designed to calculate D_{CO_2} and D_{HCO_3} from $D_{\text{H}^{\text{app}}}$ measurements. Since CO_2 diffuses 46% faster than HCO_3^- (a difference attributable to molecular size)², D_{CO_2} and D_{HCO_3} are numerically constrained to one another, reducing the system of equations to one unknown. This algorithm, described in more detail in the Supplement, performs simulations for a range of different test-values of D_{CO_2} (and D_{HCO_3}) and for each generates a predicted $D_{\text{H}^{\text{app}}}$. Least-squares best-fitting this output to the

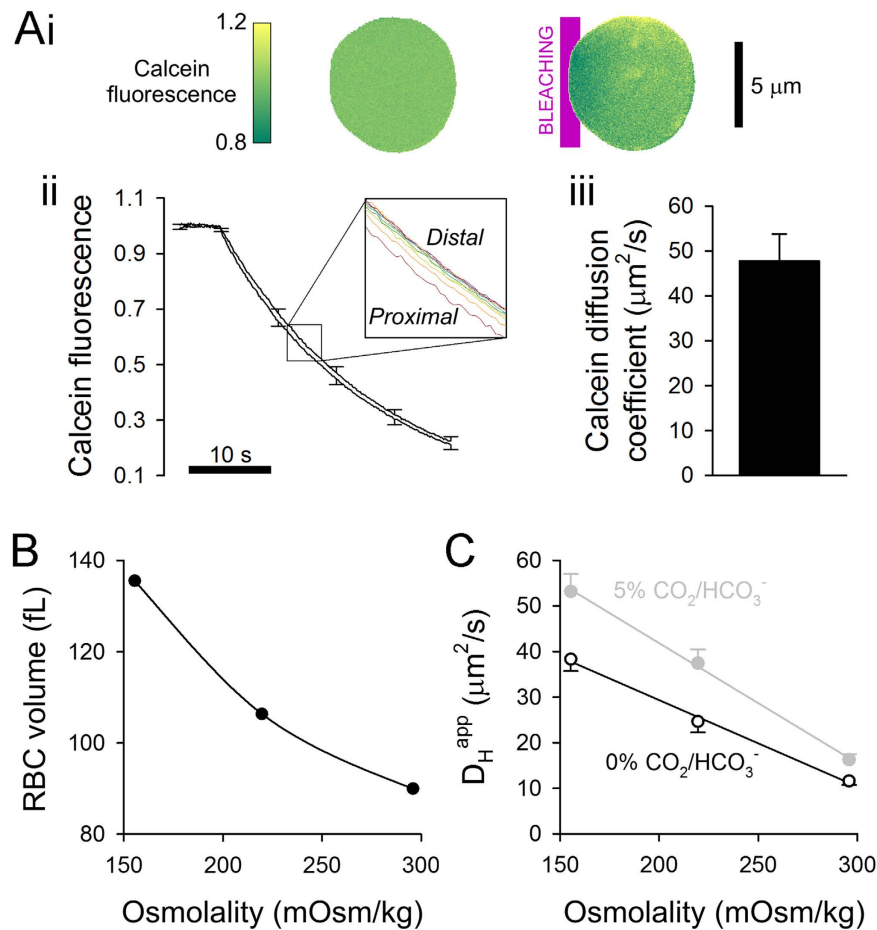


Figure 2. Hemoglobin concentration restricts cytoplasmic diffusivity. (A) Probing the diffusive tortuosity of RBC cytoplasm using calcein. (i) Localized bleaching (purple band) of calcein in intact human red blood cells (mean ± SEM of 16 cells) with a high-intensity 488 nm laser evoked a diffusive flux of calcein from non-bleached regions. Fluorescence maps normalized to the cell-averaged signal before bleaching (*left*) and after 20 s of localized bleaching (*right*). (ii) Calcein diffusivity was derived by best-fitting fluorescence time courses averaged in 10 regions of interest (ROIs; defined in the same way as for H⁺ uncaging experiments). (iii) Calcein diffusion coefficient (mean ± SEM of 16 cells). (B) Osmotic swelling of human RBCs (flow cytometry repeated thrice; >50,000 cells each) dilutes hemoglobin concentration. (C) Apparent H⁺ diffusivity ($D_{\text{H}}^{\text{app}}$) increases as hemoglobin concentration is reduced, but the relationship is steeper in the presence of CO₂/HCO₃⁻ (plus 12.5 μM DIDS), indicative of increasing diffusive freedom for CO₂/HCO₃⁻ to facilitate H⁺ mobility (mean ± SEM of 9–28 cells).

experimentally-determined $D_{\text{H}}^{\text{app}}$ derives D_{CO_2} (and $D_{\text{HCO}_3^-}$). The ‘known’ variables required to run these simulations were obtained as follows. Firstly, the concentration of hemoglobin was obtained from MCHC measurements^{20,32}, and the cytoplasmic concentration of CO₂/HCO₃⁻ was calculated using the Henderson-Hasselbalch equation from extracellular [CO₂] and [HCO₃⁻] and the measured transmembrane pH gradient. Secondly, hemoglobin reaction kinetics were assumed to be instantaneous, whereas the reactions of CO₂/HCO₃⁻ were modelled kinetically using data for CA activity, hydration and dehydration rate constants. Finally, hemoglobin-facilitated H⁺ diffusivity is equal to $D_{\text{H}}^{\text{app}}$ measured in CO₂/HCO₃⁻-free media.

Cytoplasmic D_{CO_2} and $D_{\text{HCO}_3^-}$ were found to be substantially lower than the rates measured in water (Fig. 4A) and were inversely correlated with MCHC (Figs 4B and S7). For example, CO₂ diffusivity in human RBC cytoplasm was 5% of the rate in water. The extent to which hemoglobin restricts small-molecule diffusion is substantially greater than previous estimates (inset to Fig. 4B; e.g. for human RBCs, the difference is one order of magnitude). Thus, highly restricted diffusivity of CO₂ gas and HCO₃⁻ anions in RBC cytoplasm is a hitherto unrecognized rate-limiting step in the process of gas exchange.

Discussion

Chemical reactions and membrane transport are recognized to be critically important in determining the rate of gas exchange, and their experimental characterization has informed our current model of RBC physiology. The results of this study indicate that diffusion inside RBCs is a strongly rate-limiting factor for gas turnover. We find that RBC cytoplasm is a highly tortuous environment that substantially restricts the movement of solutes,

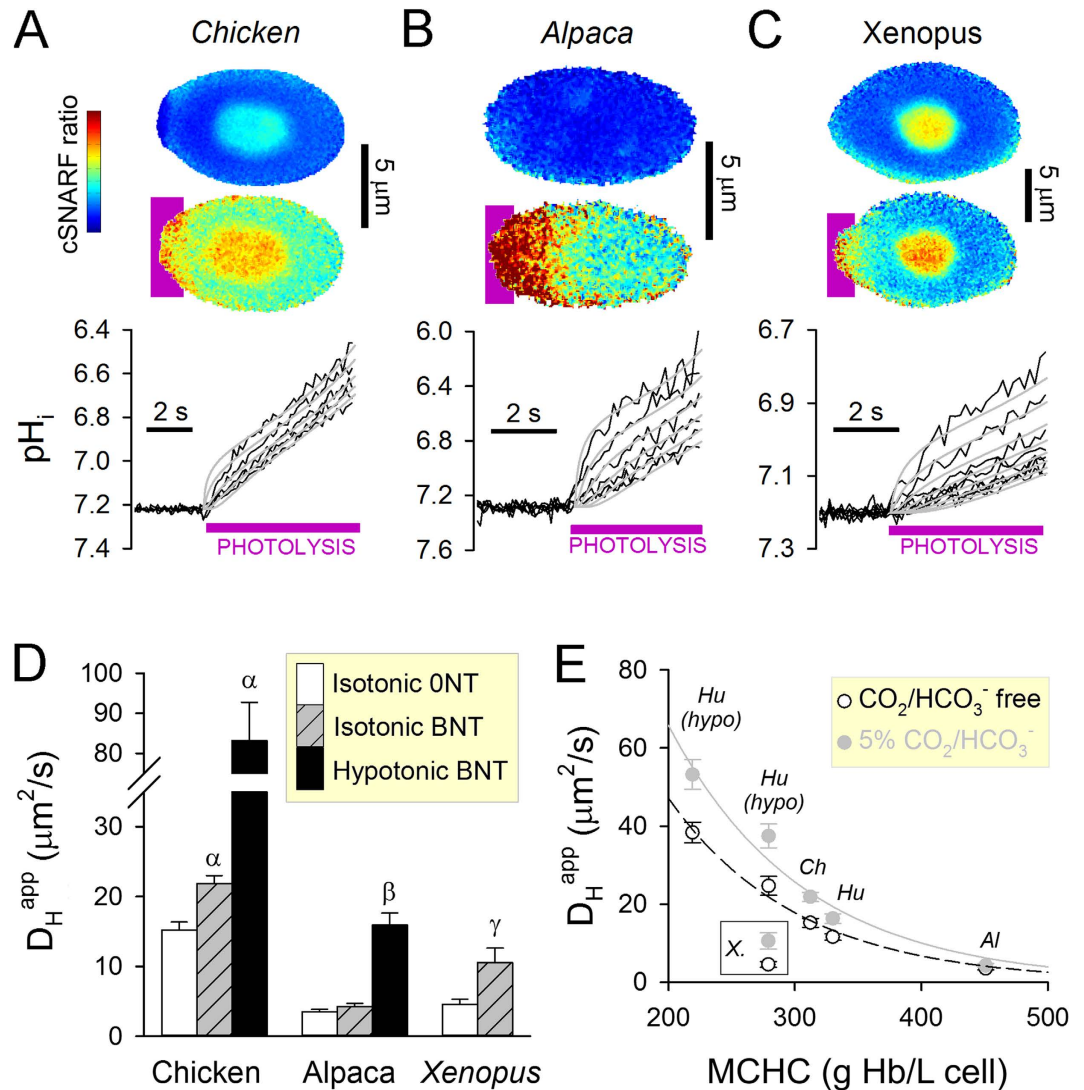


Figure 3. Measuring cytoplasmic H^+ mobility in RBCs from different animal species. (A,B) H^+ diffusion measurements in chicken and alpaca RBCs were performed according to the protocol for human RBCs (superfusate pH 7.8 and 37°C). (C) For cold-blooded *Xenopus* RBCs, superfusates were at pH 7.5 and 25°C . N.B.: For measuring fluorescence in ROIs, the signal from the nuclei was excluded. Measured pH_i time courses (black; in ROIs 1, 2, 3, 4, 5, 6, 8) are superimposed with best-fit time courses (grey), determined by the least-squares method. (D) D_H^{app} in chicken, alpaca and *Xenopus* RBCs measured in isotonic $\text{CO}_2/\text{HCO}_3^-$ -free buffer (0NT; mean \pm SEM of 14, 21, 19 cells), isotonic $\text{CO}_2/\text{HCO}_3^-$ -containing buffer (BNT; mean \pm SEM of 18, 25, 13 cells) or hypotonic BNT (mean \pm SEM of 7, 19 cells). Superfusates were at pH 7.8 and 37°C for mammals, and pH 7.5 and 25°C for *Xenopus*. Osmotic swelling increases D_H^{app} (not tested in *Xenopus* RBCs due to osmotic fragility). Symbols α , β and γ denote significance ($P < 0.0005$) compared to measurements in isotonic 0NT. (E) D_H^{app} decreases with increasing mean corpuscular hemoglobin concentration (MCHC). Hu-human, Ch-chicken, Al-alpaca, X-*Xenopus*; hypo: osmotically-swollen cells. The facilitatory effect of $\text{CO}_2/\text{HCO}_3^-$ on D_H^{app} diminishes at higher MCHC.

consistent with the uniquely high microviscosity inside RBCs³³. In terms of resistances to overall gas transport³⁴, the component attributable to RBC cytoplasm has hitherto been underestimated, and so it is plausible that the other resistances in series (imposed by membranes and extracellular unstirred layers) have been exaggerated in earlier analyses³.

The extent to which the cytoplasm of intact human RBCs restricts gas diffusion is greater than estimated previously from cell-free solutions^{12,15}. This may relate to the significantly slower rotational diffusion of hemoglobin inside RBCs compared to solution³³, which argues that encapsulation in a membrane produces a more rigid lattice of macromolecules. It is also possible that diffusivity measurements in cell-free solutions may have been over-estimated as a result of convective currents of the medium, which are much less likely to occur inside cells. Of note is that our measured effect of hemoglobin on CO_2 diffusivity is quantitatively similar to

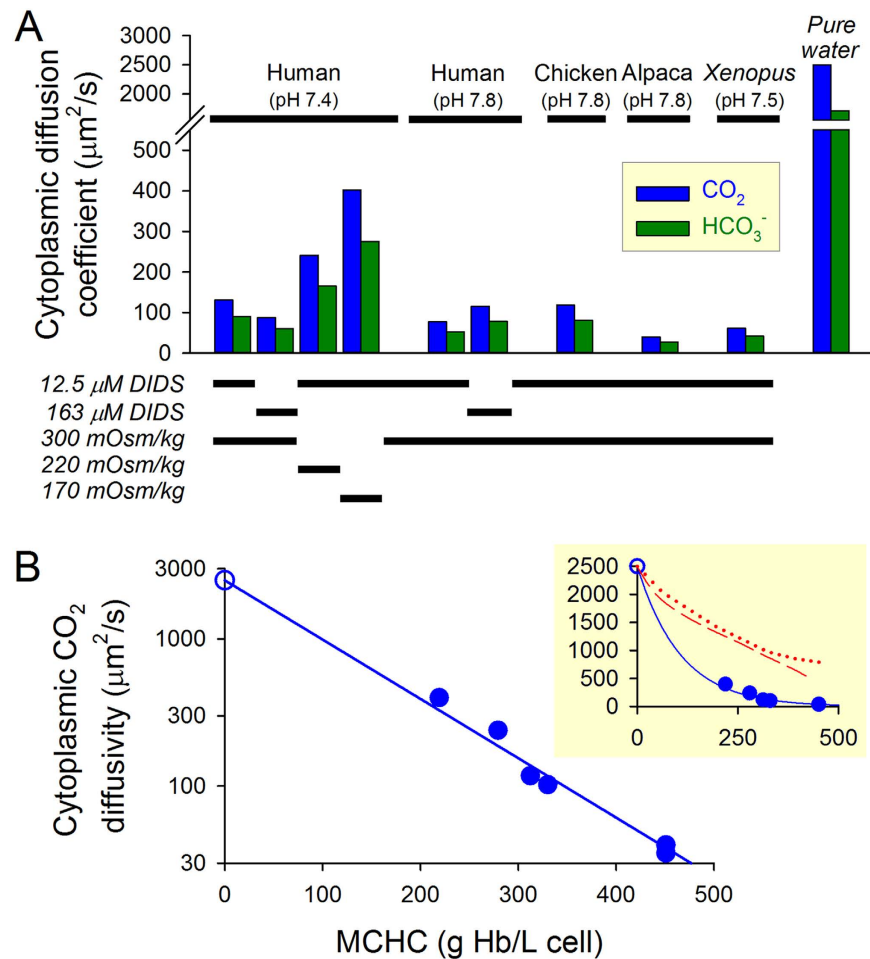


Figure 4. CO_2 diffuses slowly in RBC cytoplasm. (A) Cytoplasmic CO_2 and HCO_3^- diffusion coefficients calculated from $D_{\text{H}}^{\text{app}}$ (37°C for human, chicken and alpaca, 25°C for *Xenopus*) compared to data for pure water. (B) Cytoplasmic CO_2 diffusivity fitted to an exponentially-declining function of mean corpuscular hemoglobin concentration (MCHC). Filled circles: data from human, chicken and alpaca RBCs; open circle: data for water (all 37°C). Cytoplasmic CO_2 diffusivity halves for every 75 g/L increase in MCHC. *Inset*: plot on linear y-axis, with data from ref. 2 (dashed line) and ref. 14 (dotted line) for gas diffusion coefficients normalized to CO_2 diffusivity in water ($2500\mu\text{m}^2/\text{s}$).

the effect of an unrelated macromolecule, Ficoll70, on rhodamine green diffusion^{35,36}. Thus, hemolysates and hemoglobin-solutions may have only a limited ability to fully recapitulate the biophysical properties of intact RBC cytoplasm.

The cytoplasm of human RBCs reduces CO_2 diffusivity by a factor of 23 and calcein diffusivity by 13-fold. The difference in tortuosity imposed on CO_2 and calcein may relate to the solute's reactivity with hemoglobin. CO_2 binds weakly and reversibly to hemoglobin² (forming carbamino-hemoglobin), which will retard CO_2 translational diffusion. In contrast, the highly negatively charged calcein will not interact with hemoglobin in this way. Also, because the CO_2 molecule (radius 2 \AA) is 50-fold smaller than the calcein molecule (radius 7.4 \AA), CO_2 may be able to interact more intimately with the surface of the hemoglobin (radius 27.5 \AA). Consequently, CO_2 may experience a more tortuous path around hemoglobin, compared to calcein.

Since diffusivity, path-length and cell shape are inter-related, our measurements are an important addition to our understanding of RBC form and function. In light of highly restricted diffusivity, the advantage of flattening an RBC can be explained in terms of minimizing critical time delays, which are proportional to the square of distance. To explore this proposal, a mathematical model (described more fully in the Supplement) simulated the time course of CO_2 penetration into human RBCs entering a hypercapnic (8% CO_2) environment (Fig. 5Ai). Predictions for normal human RBCs (half-thickness $0.9\mu\text{m}$; diameter $8\mu\text{m}$) were compared to those for a hypothetical spherical variant (diameter $8\mu\text{m}$). Using D_{CO_2} data derived previously from cell-free solutions (40% of diffusivity in water, labelled here as 'fast'), the time-to-reach 90% of the equilibrium state (τ_{90}) for CO_2 partial pressure ($p\text{CO}_2$) was adequately rapid in both the flat (0.03 s) and spherical (0.09 s) geometry (Fig. 5Aii). Simulations using the presently determined value of D_{CO_2} (5% of diffusivity in water, i.e. 'slow') showed a dramatically prolonged τ_{90} for $p\text{CO}_2$ equilibration: 0.09 s for a flat RBC and 0.38 s for its spherical variant (Fig. 5Aiii). The later delay is incompatible with efficient gas exchange with faster blood flows (e.g. in exercise). Thus, the critical importance of RBC thickness for efficient gas exchange becomes apparent only when *slow* cytoplasmic diffusivity

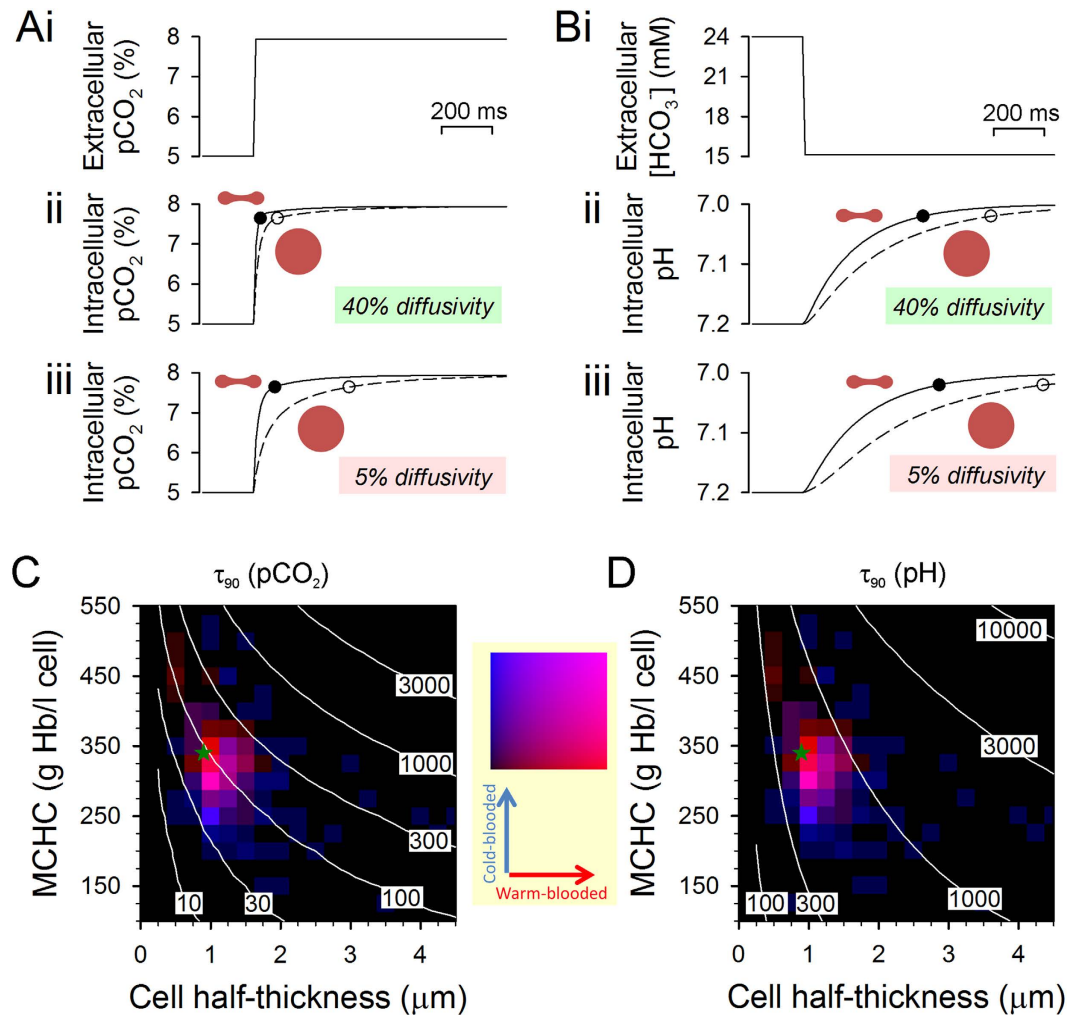


Figure 5. Results of mathematical simulations. (A) Time-to-complete 90% equilibration (τ_{90}) of $p\text{CO}_2$ inside RBC in response to an increase in ambient $[\text{CO}_2]$ (a respiratory acidosis of 7.2). (i) Extracellular $p\text{CO}_2$. (ii) Simulations with fast D_{CO_2} diffusivity: 40% of rate in water, as determined in cell-free solutions. Intracellular $p\text{CO}_2$ in a flattened human RBC (continuous line) and a hypothetical spherical version of the same diameter (dashed line). Circles indicate τ_{90} . (iii) Simulations repeated with more restricted D_{CO_2} diffusivity: at 5% of rate in water. The benefit of a flattened shape is more apparent with slow D_{CO_2} . (B) Time-to-complete 90% (τ_{90}) of acid uptake by an RBC in response to a decrease in ambient $[\text{HCO}_3^-]$ (a metabolic acidosis of 7.2). (i) Extracellular $[\text{HCO}_3^-]$. (ii) Simulations with fast D_{CO_2} for flattened (continuous line) and spherical (dashed line) cells. Circles indicate τ_{90} . (iii) Simulations repeated with more restricted D_{CO_2} . (C) Heat map showing binned data on MCHC and RBC half-thickness data from >250 species of cold- and warm-blooded animals (see inset for look-up table). Superimposed contours (units: ms) show model predictions for time-to-complete 90% equilibration τ_{90} of $p\text{CO}_2$ in RBCs, based on human RBC data modified accordingly for thickness, MCHC and hence diffusivity of CO_2 , HCO_3^- and hemoglobin. Most species fall in the range $0.03 \text{ s} < \tau_{90} < 0.3 \text{ s}$. (D) Heat map superimposed with model predictions for time-to-complete 90% (τ_{90}) acid uptake into RBCs, based on human RBC data modified accordingly for thickness, MCHC and hence diffusivity of CO_2 , HCO_3^- and hemoglobin. Most species fall in the range $0.3 \text{ s} < \tau_{90} < 1 \text{ s}$.

is considered. The cytoplasmic restrictions imposed on CO_2 movement may also apply to O_2 diffusion, therefore RBC thickness could also be important in determining the rate of O_2 exchange.

Another consequence of profoundly restricted CO_2 and HCO_3^- diffusion is very slow H^+ ion mobility in RBC cytoplasm. Remarkably, H^+ diffusivity inside RBCs is the slowest among all ions studied in cells; this is somewhat surprising given that RBCs experience the highest acid-base turnover in the body²⁶. H^+ ions are a powerful signal that regulates O_2 binding to hemoglobin through the Bohr²⁴ and Root Effects^{37,38}, but this response is only effective if the RBC's mean cytoplasmic pH (pH_{RBC}) is able to track changes in ambient pH (e.g. during the transit through acidic microvasculature of contracting muscles). Slow cytoplasmic H^+ diffusion thus places an additional constraint on RBC thickness, which was analyzed, using the model, in terms of the pH_{RBC} response to an ambient metabolic acidosis (Fig. 5Bi). Assuming the higher D_{CO_2} value, a flattened RBC will acidify faster than a spherical cell, but in both cases, τ_{90} was under 1 s (0.48 s for flat; 0.75 s for spherical; Fig. 5Bii). Using the lower D_{CO_2} value

measured herein, τ_{90} would increase to 0.54 s and 0.95 s for flat and spherical cells, respectively (Fig. 5Biii). The delay associated with spherical geometry would result in only a partial manifestation of the Bohr Effect, and consequently suboptimal distribution of O_2 to tissues. Thus, in order for O_2 release from RBCs to respond adequately to changes in ambient pH, the cell must acquire a flattened form.

Circulating human RBCs undergo a dramatic velocity-dependent deformation (e.g. parachute-like shape) as they transit through the microvasculature^{39–41}. As a result of cytoplasmic re-distribution, the intracellular diffusion distances may modestly increase towards the leading edge of the cell and decrease at rear. Nonetheless, the parachute RBC retains an overall flattened form that is compatible with efficient gas exchange. This ability of flattened human RBCs to attain a parachute shape in capillaries may be critical for maintaining minimal cytoplasmic path-lengths for efficient gas exchange.

Our work also quantified the effect of MCHC on gas diffusion. There is considerable inter-species variation in MCHC (Table S2) which, at least in part, is driven by demand for O_2 -carrying capacity, but nonetheless appears to be capped at ~ 550 g/L. High MCHC is associated with raised microviscosity and resistance to blood flow^{6,42}, which could underlie the biological limit of MCHC, although this can be compensated for by reducing RBC count. Here, we demonstrate that raising MCHC by 75 g/L halves D_{CO_2} (Fig. 4B), an effect that is quantitatively similar to that of other macromolecules (e.g. rhodamine green diffusivity halves with every 88 g/L rise in Ficoll70 concentration)³⁶. Thus, a physiological need to pack more hemoglobin into a RBC (e.g. observed in some altitude-adapted species, such as llamas and alpacas) comes at the cost of more restricted gas diffusivity. Cells adapted in this manner would need to be appropriately thinner in order to support efficient gas exchange. To investigate this hypothesis, we compiled data on RBC half-thickness (i.e. the shortest cytoplasmic path-length) and MCHC from >250 cold- and warm-blooded species (see Table S2; Fig. S8). Figure 5C shows a two-dimensional frequency histogram for RBC half-thickness and MCHC, superimposed with simulations for the time-to-reach 90% pCO_2 equilibrium (τ_{90}), determined using the model, shown in Fig. 5A, with appropriately varied MCHC (hence D_{CO_2} , D_{HCO_3}) and half-thickness. The majority of naturally-occurring MCHC/half-thickness combinations fell in the τ_{90} range of 0.03–0.3 s, i.e. compatible with near-complete equilibration during typical capillary transit times. This model was also used to simulate τ_{90} for pH_{RBC} equilibration in response to ambient acidosis. The majority of naturally-occurring MCHC/half-thickness combinations were constrained to meet the criterion of $\tau_{90} < 1$ s (Fig. 5D). We postulate that thick RBCs with high MCHC (i.e. upper right quadrant in Fig. 5C,D) are not normally found in nature because these would be associated with unacceptably slow gas exchange (τ_{90} for pCO_2 equilibration >0.3 s) and an incomplete manifestation of the Bohr Effect (τ_{90} for pH_{RBC} equilibration >1 s). Membrane tension and, in some species, the presence of a nucleus limit the extent to which RBCs could be made thinner; we propose that this imposes a cap on MCHC. According to Fig. 4B, MCHC greater than 500 g/L would restrict CO_2 diffusion by a factor of >100 , requiring RBCs to be thinner than $1 \mu m$; this may explain why such high hemoglobin levels are rare, despite pertinent selection pressures for increasing O_2 -carrying capacity. This line of reasoning may also explain why mature RBCs in mammals have lost their nucleus in a bid to become thinner.

The regulatory means by which normal RBCs meet the favorable MCHC/half-thickness criterion is likely to involve interactions within the set of gene loci (e.g. seventy-five in humans)⁴³ that collectively determine RBC shape and hemoglobin content. Failure to attain a favorable combination of cell thickness and MCHC may impact on gas exchange efficiency. The analyses shown in Fig. 5C,D highlight a potential disadvantage of attaining spherical symmetry in diseases such as hereditary spherocytosis⁴⁴, where mean cytoplasmic path-length increases due to shape and also MCHC tends to be higher due to cellular dehydration^{45,46}. These circumstances predict a less complete gas exchange and only a partial manifestation of the Bohr effect at higher blood flows, which may contribute towards the reduced exercise tolerance commonly observed in patients with hereditary spherocytosis⁴⁶.

Restricted diffusion in RBC cytoplasm may have important physiological implications besides gas exchange at capillaries. Slow diffusion of nitric oxide in RBC cytoplasm, in addition to the immobilizing effect of hemoglobin nitrosylation, may be a requirement for confining its signaling cascade to a sub-membranous domain⁴⁷. A dense network of proteins may restrict gas diffusion in non-erythroid cell types or subcellular structures⁴⁸. The magnitude of macromolecule-restricted diffusion highlights the potential for cytoplasm to regulate gas fluxes, a feat considered thus far to be in the remit of cell membranes only.

In conclusion, we propose that the efficiency of gas exchange depends critically on RBC thickness because the high density of hemoglobin restricts the movement of small solutes. This restriction is substantially greater in intact RBCs, compared to cell-free hemoglobin solutions or hemolysates, which explains why the cytoplasmic mobility of gases, HCO_3^- and H^+ ions has previously been overlooked as a rate-limiting step in the gas exchange cascade. In addition to increasing the cell's surface area/volume ratio for greater trans-membrane solute traffic and providing mechanical advantages for blood flow, the evolutionarily-conserved flattening of RBCs is an essential adaptation to minimize delays owing to slow cytoplasmic diffusion.

Methods

Red blood cells. Alpaca (*Vicugna pacos*) and chicken (*Gallus gallus*) blood were collected by trained staff from Seralabs (U.K.) and delivered on ice within 24 hours of collection. *Xenopus laevis* blood was collected by ventricular puncture of animals that have been sacrificed humanely by pithing in accordance with Schedule I of Animal (Scientific Procedures) Act 1986 carried out in a licensed facility at Oxford University. Human blood was obtained from two volunteers who gave formal and informed consent, in accordance with Central University Research Ethics Committee (CUREC) guidelines (reference: R46540/RE001, approved procedure #24), and data were fully anonymized and not traceable to the donor. All methods involving the use of blood were performed in accordance with ethical guidelines set by Oxford University, with appropriate risk assessments in place. All experimental protocols performed on collected human red blood cells are performed in accordance with Oxford University's Central University Research Ethics Committee (CUREC) guidelines (reference: R46540/RE001,

approved procedure #24). Additionally, all experimental protocols performed on animal and human red blood cells were performed in accordance with Oxford University's Health and Safety regulations (OHS Policy Documents 1/03, 1/01, OHS 2/03, UGN S1/95). Clinical tests confirmed that mean corpuscular volume (MCV) and mean corpuscular hemoglobin concentration (MCHC) of donor blood were in the normal range (MCV: 88.2–90.9 fL, MCHC: 325–334 g/L). Blood samples were collected in tubes treated with heparin (*Xenopus*) or EDTA (all other species), spun-down at 4 °C (10,000 for 5 min for mammalian blood; 5,000 for 5 min for chicken blood; 1,000 for 10 min for *Xenopus* blood) to remove the supernatant and buffy coat. A sample of the fraction containing packed red blood cells was re-suspended in Hepes-buffered NT and used for confocal imaging or flow cytometry; the remainder was freeze-thawed twice to break up cell membranes, and used for measurements of hemoglobin concentration (HemoCue Hb 201plus), histidyl-containing small molecules (Pauly's assay) and carbonic anhydrase activity.

Confocal imaging. To image intracellular pH (pH_i), cells were loaded with the acetoxymethyl (AM) ester of the pH-reported dye cSNARF1 for 60 minutes (*Xenopus*) or 10 minutes (all other species), and allowed to settle on a poly-L-lysine pretreated coverslip at the base of a superfusion chamber mounted on an inverted Zeiss Axiovert microscope that was coupled to a Zeiss LSM700 confocal system. Superfusates were delivered at 4 mL/min at 25 °C (*Xenopus*) or 37 °C (all other species). Cells were imaged with a x100 objective and stored as stacks of 256 × 256 pixel 8-bit bitmaps (53 nm pixel length). cSNARF1 was excited by a 555 nm laser line and fluorescence was collected at 580 ± 10 and 640 ± 10 nm. The fluorescence ratio was converted to pH using a calibration curve, obtained by a published method²⁰. To image calcein, cells were loaded with calcein-AM for 10 minutes, and fluorescence (>515 nm) was excited with low intensity 488 nm laser line. Offline analysis was performed using ImageJ.

H⁺ uncaging and calcein bleaching. Photolytic uncaging of H⁺ ions from 6-nitroveratraldehyde²³ (NVA; added to solutions at 1 mM) was evoked by scanning a region of interest (ROI) at one end of the RBC (ROI width equal to 1/10th of RBC diameter) with 405 nm laser light, as shown in Fig. 1C,D. By alternating between regional H⁺ uncaging and whole-field pH_i -imaging, the spatial dissipation of H⁺ ions from the uncaging site can be followed. Fluorescence maps were analyzed using ImageJ. Two stacks of images (580 nm and 640 nm fluorescence) were background-offset and fluorescence signal was averaged in ten ROIs of width equal to 1/10th of the RBC diameter along x-axis and height equal to the RBC diameter in the y-axis. For *Xenopus* and chicken, the fluorescence from the nucleus was excluded from analysis. ROI1 represented the uncaging region. The ratio of ROI fluorescence at 580 and 640 nm was converted to [H⁺] time courses, which were fitted with a diffusion equation to obtain the apparent diffusion coefficient (D_H^{app}), according to an algorithm described previously²⁶ and in the Supplement. Bleaching of calcein fluorescence was performed by a similar protocol to H⁺ uncaging. The excitation protocol alternated between high intensity laser for localized calcein bleaching and low intensity 488 nm laser for imaging cytoplasmic calcein. Time courses of calcein fluorescence, measured in ten ROIs, were fitted with a diffusion equation, similar to that described in the Supplement for analyzing D_H^{app} .

References

- Wagner, P. D. Diffusion and chemical reaction in pulmonary gas exchange. *Physiol Rev* **57**, 257–312 (1977).
- Geers, C. & Gros, G. Carbon dioxide transport and carbonic anhydrase in blood and muscle. *Physiol Rev* **80**, 681–715 (2000).
- Endeward, V. & Gros, G. Extra- and intracellular unstirred layer effects in measurements of CO₂ diffusion across membranes—a novel approach applied to the mass spectrometric 18O technique for red blood cells. *J Physiol* **587**, 11531167 (2009).
- Fedosov, D. A., Pan, W., Caswell, B., Gompper, G. & Karniadakis, G. E. Predicting human blood viscosity in silico. *Proc Natl Acad Sci USA* **108**, 11772–11777 (2011).
- Uzoigwe, C. The human erythrocyte has developed the biconcave disc shape to optimise the flow properties of the blood in the large vessels. *Med Hypotheses* **67**, 1159–1163 (2006).
- Chien, S. Red cell deformability and its relevance to blood flow. *Annu Rev Physiol* **49**, 177–192 (1987).
- Noguchi, H. & Gompper, G. Shape transitions of fluid vesicles and red blood cells in capillary flows. *Proc Natl Acad Sci USA* **102**, 14159–14164 (2005).
- Lim, H. W. G., Wortis, M. & Mukhopadhyay, R. Stomatocyte-discocyte-echinocyte sequence of the human red blood cell: evidence for the bilayer-couple hypothesis from membrane mechanics. *Proc Natl Acad Sci USA* **99**, 16766–16769 (2002).
- Grebe, R. & Zuckermann, M. J. Erythrocyte shape simulation by numerical optimization. *Biorheology* **27**, 735–746 (1990).
- Guest, M. M., Bond, T. P., Cooper, R. G. & Derrick, J. R. Red Blood Cells: Change in Shape in Capillaries. *Science* **142**, 1319–1321 (1963).
- Canham, P. B. The minimum energy of bending as a possible explanation of the biconcave shape of the human red blood cell. *J Theor Biol* **26**, 61–81 (1970).
- Pivkin, I. V. *et al.* Biomechanics of red blood cells in human spleen and consequences for physiology and disease. *Proc Natl Acad Sci USA* **113**, 7804–7809 (2016).
- Holland, R. A. & Forster, R. E. The effect of size of red cells on the kinetics of their oxygen uptake. *J Gen Physiol* **49**, 727–742 (1966).
- Vandegriff, K. D. & Olson, J. S. Morphological and physiological factors affecting oxygen uptake and release by red blood cells. *J Biol Chem* **259**, 12619–12627 (1984).
- Jones, D. A. The important of surface area/volume ratio to the rate of oxygen uptake by red cells. *J Gen Physiol* **74**, 643–646 (1979).
- Gros, G. & Moll, W. The diffusion of carbon dioxide in erythrocytes and hemoglobin solutions. *Pflugers Arch* **324**, 249–266 (1971).
- Spitzer, K. W., Skolnick, R. L., Peercy, B. E., Keener, J. P. & Vaughan-Jones, R. D. Facilitation of intracellular H(+) ion mobility by CO(2)/HCO(3)(-) in rabbit ventricular myocytes is regulated by carbonic anhydrase. *J Physiol* **541**, 159–167 (2002).
- Swietach, P., Spitzer, K. W. & Vaughan-Jones, R. D. pH-Dependence of extrinsic and intrinsic H(+) ion mobility in the rat ventricular myocyte, investigated using flash photolysis of a caged-H(+) compound. *Biophys J* **92**, 641–653 (2007).
- Stewart, A. K., Boyd, C. A. & Vaughan-Jones, R. D. A novel role for carbonic anhydrase: cytoplasmic pH gradient dissipation in mouse small intestinal enterocytes. *J Physiol* **516** (Pt 1), 209–217 (1999).
- Swietach, P. *et al.* Hydrogen ion dynamics in human red blood cells. *J Physiol* **588**, 4995–5014 (2010).
- Irving, M., Maylie, J., Sizto, N. L. & Chandler, W. K. Intracellular diffusion in the presence of mobile buffers. Application to proton movement in muscle. *Biophys J* **57**, 717–721 (1990).

22. Junge, W. & McLaughlin, S. The role of fixed and mobile buffers in the kinetics of proton movement. *Biochim Biophys Acta* **890**, 1–5 (1987).
23. Hulikova, A. *et al.* Stromal uptake and transmission of acid is a pathway for venting cancer cell-generated acid. *Proc Natl Acad Sci USA* (2016).
24. Bohr, C., Hasselbalch, K. & Krogh, A. Über einen in biologischer Beziehung wichtigen Einfluss, den die Kohlensäurespannung des Blutes auf dessen Sauerstoffbindung übt. *Skand Arch Physiol* **16**, 401–412 (1904).
25. Swietach, P. & Vaughan-Jones, R. D. Relationship between intracellular pH and proton mobility in rat and guinea-pig ventricular myocytes. *J Physiol* **566**, 793–806 (2005).
26. Swietach, P. *et al.* Modelling intracellular H(+) ion diffusion. *Prog Biophys Mol Biol* **83**, 69–100 (2003).
27. Gros, G. *et al.* Evidence for rotational contribution to protein-facilitated proton transport. *Proc Natl Acad Sci USA* **81**, 1710–1714 (1984).
28. Vanysek, P. In *CRC Handbook of Chemistry and Physics* (ed D. R. Linde) Ch. 5, 93–95 (CRC Press, 1999).
29. Seely, J. E. & Marshall, F. D. Carnosine levels in blood. *Experientia* **37**, 1256–1257 (1981).
30. Richards, M. *et al.* Intracellular tortuosity underlies slow cAMP diffusion in adult ventricular myocytes. *Cardiovasc Res* **110**, 395–407 (2016).
31. Van Balgooy, J. N., Marshall, F. D. & Roberts, E. Carnosine in nucleated erythrocytes. *Nature* **247**, 226–227 (1974).
32. Cass, A. & Dalmark, M. Equilibrium dialysis of ions in nystatin-treated red cells. *Nat New Biol* **244**, 47–49 (1973).
33. Wang, D., Kreutzer, U., Chung, Y. & Jue, T. Myoglobin and hemoglobin rotational diffusion in the cell. *Biophys J* **73**, 2764–2770 (1997).
34. Cooper, G. J., Occhipinti, R. & Boron, W. F. CrossTalk proposal: Physiological CO₂ exchange can depend on membrane channels. *J Physiol* **593**, 5025–5028 (2015).
35. Dauty, E. & Verkman, A. S. Molecular crowding reduces to a similar extent the diffusion of small solutes and macromolecules: measurement by fluorescence correlation spectroscopy. *J Mol Recognit* **17**, 441–447 (2004).
36. Dix, J. A. & Verkman, A. S. Crowding effects on diffusion in solutions and cells. *Annu Rev Biophys* **37**, 247–263 (2008).
37. Rummer, J. L., McKenzie, D. J., Innocenti, A., Supuran, C. T. & Brauner, C. J. Root effect hemoglobin may have evolved to enhance general tissue oxygen delivery. *Science* **340**, 1327–1329 (2013).
38. Riggs, A. F. The Bohr effect. *Annu Rev Physiol* **50**, 181–204 (1988).
39. Shelby, J. P., White, J., Ganesan, K., Rathod, P. K. & Chiu, D. T. A microfluidic model for single-cell capillary obstruction by Plasmodium falciparum-infected erythrocytes. *Proc Natl Acad Sci USA* **100**, 14618–14622 (2003).
40. Tomaiuolo, G. & Guido, S. Start-up shape dynamics of red blood cells in microcapillary flow. *Microvasc Res* **82**, 35–41 (2011).
41. Tomaiuolo, G. Biomechanical properties of red blood cells in health and disease towards microfluidics. *Biomicrofluidics* **8**, 051501 (2014).
42. Fedosov, D. A., Noguchi, H. & Gompper, G. Multiscale modeling of blood flow: from single cells to blood rheology. *Biomech Model Mechanobiol* **13**, 239–258 (2014).
43. van der Harst, P. *et al.* Seventy-five genetic loci influencing the human red blood cell. *Nature* **492**, 369–375 (2012).
44. Reinhart, W. H. & Chien, S. Red cell rheology in stomatocyte-echinocyte transformation: roles of cell geometry and cell shape. *Blood* **67**, 1110–1118 (1986).
45. Cynober, T., Mohandas, N. & Tchernia, G. Red cell abnormalities in hereditary spherocytosis: relevance to diagnosis and understanding of the variable expression of clinical severity. *J Lab Clin Med* **128**, 259–269 (1996).
46. Perrotta, S., Gallagher, P. G. & Mohandas, N. Hereditary spherocytosis. *Lancet* **372**, 1411–1426 (2008).
47. Pawloski, J. R., Hess, D. T. & Stamler, J. S. Export by red blood cells of nitric oxide bioactivity. *Nature* **409**, 622–626 (2001).
48. Waisbren, S. J., Geibel, J. P., Modlin, I. M. & Boron, W. F. Unusual permeability properties of gastric gland cells. *Nature* **368**, 332–335 (1994).

Acknowledgements

Supported by a Royal Society fellowship to P.S. We thank Colin Akerman and Mala Rohling for supplying *Xenopus* blood, and Alzbeta Hulikova for assistance with Pauly's assay.

Author Contributions

S.L.R. performed and analyzed experiments. P.S. designed the research and wrote the manuscript.

Additional Information

Supplementary information accompanies this paper at <http://www.nature.com/srep>

Competing financial interests: The authors declare no competing financial interests.

How to cite this article: Richardson, S. L. and Swietach, P. Red blood cell thickness is evolutionarily constrained by slow, hemoglobin-restricted diffusion in cytoplasm. *Sci. Rep.* **6**, 36018; doi: 10.1038/srep36018 (2016).



This work is licensed under a Creative Commons Attribution 4.0 International License. The images or other third party material in this article are included in the article's Creative Commons license, unless indicated otherwise in the credit line; if the material is not included under the Creative Commons license, users will need to obtain permission from the license holder to reproduce the material. To view a copy of this license, visit <http://creativecommons.org/licenses/by/4.0/>

© The Author(s) 2016